ANL/XFD/CP-97774

Resonant Raman Scattering in Nd_2O_3 and the Electronic Structure of Sr_2RuO_4 Studied by Synchrotron Radiation Excitation

D.L. Ederer,[1*] A. Moewes,[2] E.Z. Kurmaev,[3] T.A. Callcott,[4] M.M. Grush[4], S. Stadler,[5†] R. Winarski,[5] R.C.C. Perera,[6] and L.J. Terminello[7]

[1]Advanced Photon Source, Argonne National Laboratory, Argonne, IL 60439
[2]Center for Advanced Microstructures and Devices, Baton Rouge, LA 70888
[3]Institute of Metal Physics, Russian Academy of Sciences-Ural Division, 620219 Yekaterinburg GSP-170, Russia
[4]University of Tennessee, Knoxville, TN 37996
[5]Tulane University, New Orleans, LA 70118
[6]Advanced Light Source, Lawrence Berkeley Laboratory, Berkeley, CA 94720
[7]Lawrence Livermore National Laboratories Livermore, CA 94551

RECEIVED
SEP 28 1999
OSTI

November 5, 1998

Abstract. This paper is intended to illustrate two points. The first being the extensive growth of resonant Raman soft x-ray scattering due to the emergence of third-generation x-ray sources. With these sources, the ubiquitous presence of Raman scattering near the 3d and 4d ionization thresholds has been used to elucidate the excitation process in a number of rare earth and transition metal compounds. Such scattering can produce dramatic changes in the emission spectrum, as we show in our example of inelastic scattering at the 3d threshold of Nd_2O_3. Photon-in photon-out soft x-ray spectroscopy is adding a new dimension to soft x-ray spectroscopy by providing many opportunities for exciting research, especially at third-generation synchrotron light sources. Second, it is very effective to use theory and experiment to characterize the electronic properties of materials. In particular we confirmed in-plane oxygen-ruthenium bonding in Sr_2RuO_4, this first copperless perovskite superconductor, by analyses using calculations, soft x-ray emission spectroscopy (SXE) and photoelectron spectroscopy (PES). Measurements of this type illustrate the importance of combining SXE and PES measurements with theoretical calculations.

Keywords: Soft x-ray spectroscopy, x-ray fluorescence, Raman scattering, rare earth materials, transition metals, photoelectron spectroscopy, density of states

*Permanent address: Tulane University, New Orleans, LA 70118
†Permanent address: Naval Research Laboratory, Washington, D.C. 20021

The submitted manuscript has been authored by a contractor of the U.S. Government under contract No. W-31-109-ENG-38. Accordingly, the U.S. Government retains a nonexclusive, royalty-free license to publish or reproduce the published form of this contribution, or allow others to do so, for U.S. Government purposes.

DISCLAIMER

This report was prepared as an account of work sponsored by an agency of the United States Government. Neither the United States Government nor any agency thereof, nor any of their employees, make any warranty, express or implied, or assumes any legal liability or responsibility for the accuracy, completeness, or usefulness of any information, apparatus, product, or process disclosed, or represents that its use would not infringe privately owned rights. Reference herein to any specific commercial product, process, or service by trade name, trademark, manufacturer, or otherwise does not necessarily constitute or imply its endorsement, recommendation, or favoring by the United States Government or any agency thereof. The views and opinions of authors expressed herein do not necessarily state or reflect those of the United States Government or any agency thereof.

DISCLAIMER

Portions of this document may be illegible in electronic image products. Images are produced from the best available original document.

INTRODUCTION

Soft x-ray emission spectroscopy has been applied extensively toward the study of materials since the discovery of x-rays [1-4]. Soft x-rays are especially powerful as a probe to study bulk electronic structure, because they are atomic site specific, penetrate tens to hundreds of atomic layers, and produce less damage than electrons or ions[5]. The large penetration depth of x-rays make them an important tool to probe multilayers and atoms at buried interfaces[6]. The dipole selection rule allows one to obtain a selected localized density of states of one of the elements in the compound under investigation; thus, one obtains complimentary information to that obtained by photoelectron spectroscopy. X-ray scattering is also an important tool for investigating electronic excitations and electronic ground-state properties of many electron systems. More recently the advent of third generation sources has given researchers additional impetus to study biological systems and other materials by x-ray diffraction and by anomalous and small angle x-ray scattering. Much of this enormous body of work is summarized in several volumes of the Handbook of Synchrotron Radiation [7], and was published in the proceedings of several workshops devoted to this topic[8,9]. The advent of third generation sources has allowed scientists to extend the energy range of inelastic x-ray scattering to include the soft x-ray region of the spectrum, and several groups have studied many different materials and compounds.[5,10-12]

The processes of photon absorption and photon emission are driven by the first order process coupling the electron momentum, **p**, to the vector potential of the photon field, **A.** Weaker two photon processes involving the (**A**• **A**) term produce elastic scattering (Rayleigh scattering) and inelastic scattering (Raman and Compton scattering). Non resonant Raman scattering was observed in the x-ray spectra region three decades ago [13]. These pioneering measurements required exposing the photographic plates for about twenty-four hours to observe the x-ray scattering. Resonant Raman scattering involving the $(\mathbf{p}\bullet\ \mathbf{A})^2$ term of the Hamiltonian was observed over twenty-five years ago in the keV region of the x-ray spectrum [14-16]. The importance of these coupled scattering processes has become much more evident.

The general relationship for the scattering cross section as a function of the input photon and the scattered photon is given by the generalized Kramers-Heisenberg (K-H) equation, derived from second-order time-dependent perturbation theory 17], as shown in Eq. 1.

$$\frac{d\sigma(\upsilon_1,\upsilon_2)}{d\Omega} = r_e^2 \frac{\upsilon_2}{\upsilon_1} \sum_F \left| \langle F | e^{i(k_1 - k_2)\bullet r} | I \rangle + \frac{1}{m_e} \sum_\eta \frac{\langle F | p \bullet \varepsilon_2 | \eta \rangle \langle \eta | p \bullet \varepsilon_1 | I \rangle}{E_\eta - E_I - h\nu_1 - i\Gamma_\eta/2} + \right.$$
$$\left. \frac{1}{m_e} \sum_\eta \frac{\langle F | p \bullet \varepsilon_1 | \eta \rangle \langle \eta | p \bullet \varepsilon_2 | I \rangle}{E_\eta - E_I + h\nu_1} \right|^2 \times \delta(E_F - E_I + h\nu_1 - h\nu_2) \quad (1)$$

In this equation the first term is the Compton, non-resonant Raman and Rayleigh scattering, the second term describes resonant scattering, and the third term does not contribute significantly to the scattering amplitude and is neglected. The scaling factor for the inelastic scattering cross section is the square of the classical radius of the electron, r_e, which has a magnitude of $7.0 \times 10^{-24} cm^2$. The delta function in the K-H equation insures the conservation of energy in the scattering process. The indices, I and F, represent the initial and final states, respectively. The energy of the input photon is $h\nu_1$. The quantities $\mathbf{e_1}$ and $\mathbf{e_2}$ are the polarization directions, and $\mathbf{k_1}$ and $\mathbf{k_2}$ are the propagation directions of the input and output photons, respectively. The energies E_η and E_I are the energy of the intermediate state, η, and the energy of the initial state, respectively. The amplitudes are summed over the intermediate states, η, and the cross section is summed over the final states, F.

In the soft x-ray spectral energy region of interest, this cross section is small compared to the first-order photoionization processes, and only the resonant term contributes significantly to the scattering. The resonant scattering is characterized by a summation over the intermediate states, [18,19] thus Eq. 1 reduces to:

$$\frac{d\sigma(\upsilon_1,\upsilon_2)}{d\Omega} = r_e^2 \frac{\upsilon_2}{\upsilon_1} \frac{1}{m_e} \sum_F \left| \sum_\eta \frac{\langle F | p \bullet \varepsilon_2 | \eta \rangle \langle \eta | p \bullet \varepsilon_1 | I \rangle}{E_\eta - E_I - h\nu_1 - i\Gamma/2} \right|^2 \cdot \delta(E_F + h\nu_2 - E_I - h\nu_1) \quad (2)$$

This scattering is not limited to atomic levels but has been observed to modify the band emission of solids near threshold. The phenomena was explained by Ma *et al.* [20] as a process that involved not only energy conservation, i.e., $h\nu_1 - h\nu_2 = E_F - E_I$, but crystal momentum conservation as well so that two equations apply in solids, namely:

$$h\nu_1 - h\nu_2 = E_c(\kappa_c) - E_v(\kappa_v), \quad (3)$$

$$\mathbf{q_1} + \kappa_v = \kappa_c + \mathbf{q_2} = \mathbf{G}. \quad (4)$$

In these expressions the quantities $E_c(\kappa_c)$ and $E_v(\kappa_v)$ are the conduction band and valence band binding energies indexed to the crystal momentum vectors κ_c and κ_v of the conduction band and the valence band electron, respectively. Thus, Raman scattering can involve states localized in real

or momentum space. A number of experiments where Raman scattering from states localized in momentum space [20-25] have been performed, and some of them will be discussed by Shirley at this conference.

The advent of third-generation sources has spawned a great deal of work on resonant Raman scattering in the soft x-ray region of the spectrum, especially with rare earths and transition metals. A partial list of the materials that have been studied in the past few years, and the publication reference is given in Table I [26-40]. We shall provide an illustration taken from one of these studies to show how Raman scattering can be used to elucidate the atomic properties of neodymium [39]. We will also present recent work [41] invoking conventional incoherent x-ray excitation and show its use in the interpretation of band structure and the determination of the electronic properties of a relatively complex solid.

INSTRUMENTATION

Until recently, the exploitation of photon-excited soft x-ray emission spectroscopy in the soft x-ray range (50 eV to 1000 eV) as an extremely powerful and useful technique to study the electronic structure of atoms in solids and molecules has been limited by the small fluorescence yields (10^{-3}-10^{-4}) of materials with a low atomic number and by inefficient soft x-ray spectrometers. To counter the deficiency of low yield and low spectrometer efficiency, improved soft x-ray grating spectrometers [42,43] with sensitivities 10^3-10^4 times greater than conventional spectrometers have been coupled with third-generation synchrotron radiation sources. For the first time a narrow band of x-ray radiation ($E/\Delta E \geq 1000$) can be used to excite soft x-ray emission in its entire spectral range. This combination allows high-quality spectra to be obtained from some elemental samples [44] in about thirty seconds.

At present we employ a spectrometer mounted on a beam line at the center for Advanced Microstructures and Devices (CAMD) [45] at Louisiana State University and another spectrometer end station on an undulator at the Advanced Light Source (ALS) [44] at Lawrence Berkeley National Laboratory. The soft x-rays from the sample are energy analyzed by a grating spectrometer and a computer-interfaced multichannel detector [42]. While the apparatus we use does not rotate about the x-ray beam, the ability to rotate the spectrometer allows the experimenter to study the angular distribution of the fluorescence radiation that has been excited by either S or P polarized x-rays [34], allowing one to study the bonding orbitals in a single crystal or at surfaces. Typically, the energy resolution employed while measuring the spectra presented in the figures was between 0.3 eV and 3.3 eV.

RESULTS

Photon-in photon-out soft x-ray spectroscopy is adding many opportunities for exciting research at third-generation synchrotron light sources. Dramatic changes in the emission spectrum are observed near the 3d ionization thresholds of the rare earths due to resonant Raman scattering and Coster-Kronig processes, as we show in our example of spectra obtained in Nd_2O_3 [39]. In the second example, effective use [41] of theory and experiment is made to characterize the electronic properties of Sr_2RuO_4, the first copperless perovskite superconductor.

I) Probing electron correlation, charge transfer and Coster-Kronig transitions at the 3d and 4d thresholds of Nd by resonant inelastic scattering

The motivation to study Nd_2O_3 was to see if a purely atomic model for the emission involving 4f electrons is viable as an alternative approach to the Anderson-Impurity model. At and below the excitation threshold of the 3d electrons, the emission is dominated by inelastic scattering. Our results indicate strong Coster-Kronig decay of the $3d_{3/2}$ hole, as well as additional occupancy of the 4f level via charge transfer from the oxygen valence band only for the 3d-4f threshold. The Coster-Kronig process is an Auger decay of a core hole where the initial electron and one of the final state electrons come from the same shell. The other final state electron may come from any shell that is energetically possible. Strong inelastic scattering produces energy losses of 2.3 and 21 eV, which are due to 4f inner shell excitations ($4f^3 \rightarrow (4f^3)^*$) and 5p-4f excitations ($5p^6 4f^3 \rightarrow 5p^5 4f^4$), respectively. The results are explained by our atomic calculations indicating strong localization of the 4f electrons and suggesting that correlation effects of the 4f electrons are weak.

In Fig. 1 the x-ray emission spectrum (XES) of Nd_2O_3 above the 3d-4f threshold is displayed. The excitation energy is 1022.4 eV. Six peaks are resolved and labeled as A through F. To identify the features, we have calculated the atomic transition rates for Nd^{3+} by using Cowan's code [46]. The scaling factor for the Slater integrals [47] was 80%, and the results are shown below the XES spectrum. The calculated spectra in Fig. 1 have been broadened by 3.3 eV full width-half maximum, which is approximately the theoretical resolution of the spectrometer. Transitions between three different electron configurations were calculated, and each one is displayed in a different line style in Fig. 1. All peaks are due to the filling of the 3d hole, and the assignments are as follows:

Peak A: $3d^9\,5p^6\,4f^4\,\underline{L}\,[^6K \text{ or } 3d_{5/2}] \rightarrow 3d^{10}\,5p^5\,4f^4\,\underline{L}\,[^6I]$, (dotted line).

Peak B and D: $3d^9\,5p^6\,4f^3\,[^3G] \rightarrow 3d^{10}\,5p^5\,4f^3\,[^3F]$, (dashed line).

Peak C and E: $3d^9\,5p^6\,4f^4\,\underline{L}$ [C: $^4K_{11/2}$ or $3d_{5/2}$, E: $^4H_{7/2}$ or $3d_{3/2}$] $\rightarrow 3d^{10}\,5p^6\,4f^3\,\underline{L}\,[^4I_{9/2}]$, (solid line).

The terms corresponding to the strongest transitions between the electron configurations are given in brackets. Both **L•S** and j-j notation will be used for the terms of the configurations in this paper. The quantity $\underline{L}$ denotes a ligand hole.

In Nd_2O_3 the Nd atom is triply ionized, and the electron configuration is $3d^{10}\ 5p^6\ 4f^3$ with a $^4I_{9/2}$ ground state term. The electron configuration for the intermediate state, leading to peaks A, C and E, has four electrons in the 4f shell. Charge-transfer processes provide additional occupancy of the 4f level when exciting above the 3d absorption threshold. Charge transfer electrons from the oxygen valence band can shake down to the 4f levels from where the 3d hole can be filled. This behavior has been observed in other rare earth materials [40, 48]. Our calculations show also that peak C has some contribution from the transitions that lead to peak A (dotted line). Our data are not corrected for self-absorption because of the uncertainty of the relevant cross sections. The amplitudes of peaks C and E are diminished by self-absorption. Peak F is due to an inelastic loss.

The absorption of Nd_2O_3 in the region of the 3d threshold has been measured by detecting the total electron yield (TEY), and the spectrum is displayed in Fig. 1. The features mainly arise from excitations of the $3d^{10}\ 4f^3$ ($^4I_{9/2}$) ground state to the $^4K_{11/2}$ ($3d_{5/2}$) and $^6K_{9/2}$, $^4I_{9/2}$ and $^4H_{7/2}$ ($3d_{3/2}$) terms of the $3d^9\,4f^4$ configuration. The measured spectrum for Nd_2O_3 is well reproduced in detail including the relative peak height by the calculation for atomic Nd^{3+}. This indicates the strong localization of the 4f electrons.

Fig. 1 also exhibits the measured partial fluorescence yield (PFY) of Nd_2O_3. It represents the total intensity emitted in the detectable range (880-1100 eV) versus photon excitation energy. Two differences in electron (TEY) and fluorescence yield (PFY) spectra, are apparent: The energetic position of the $3d_{5/2}$ is not the same for the two spectra and the peaks are much broader in the fluorescence yield spectrum. We will discuss this after introducing the next figure.

In Fig. 2 the measured emission spectra for Nd_2O_3 are shown for various excitation energies through the 3d-4f thresholds. Above the $3d_{3/2}$ threshold (998.6 eV), the spectra display the four fluorescence features as discussed above. The spectrum taken at an excitation energy of 1022.4 eV is the same XES spectrum as displayed in Fig.1. We note in passing, that some details cannot been seen clearly because of the large number of spectra displayed. This is due to the extended scale used in Fig. 2. At and below the $3d_{3/2}$ threshold, the fluorescence evolves into inelastic scattering. Resonant inelastic scattering dominates the emission process, and we observe two inelastic loss features at 2.3 and 21 eV. The loss features corresponding to a constant energy loss of 2.3 eV are due to 4f inner shell excitations $4f^3 : {}^4I_{9/2} \rightarrow (4f^3)^* : {}^4G_J$, ^2H_J and ^2G_J through the $^4H_{7/2}$ intermediate states of the $3d^9 4f^4$ electron configuration. These so-called "f-f-transitions" are typical for rare

earth materials and have been observed recently for the first time in Gd [35]. The loss features at an energy loss of 21 eV are due to net transitions in which a 5p electron is promoted into the 4f shell $3d^9 5p^6 4f^3 \rightarrow 3d^9 5p^6 4f^4 \rightarrow 3d^9 5p^5 4f^4$. These interpretations are discussed in more detail and with calculation of the energy loss spectra elsewhere [39].

Comparison of the XES spectra (Fig. 2) and the partial fluorescent yield (Fig. 1) shows that inelastic processes dominate the emission from the sample, especially near the 3d absorption thresholds. This behavior has been observed in La as well [40]. The dominating inelastic scattering accounts for the fact that the features in partial fluorescence (PFY in Fig. 1) are broader than in absorption (TEY in Fig. 1) and suggests the intermediate state lifetime for fluorescence is short compared to the lifetime for total absorption. The inelastic scattering also accounts for the different energetic position of the peaks in TEY and PFY spectra. Fluorescence from the decay of the $3d_{5/2}$ hole (peaks A, B and C in Fig. 1) is observed after creating the $3d_{3/2}$ hole (excitation energies of greater than 998.6 eV). This indicates strong Coster-Kronig decay of the $3d_{3/2}$ hole of the kind $3d_{3/2} \rightarrow 3d_{5/2}$. When exciting at the $3d_{5/2}$ threshold directly (976.4 eV), only the fluorescence from the decay of the $3d_{5/2}$ is apparent (peaks A and C).

Our atomic calculations are in excellent agreement with the experimental results emphasizing the localized character of the 4f electrons. The emission of rare earth systems with fewer 4f electrons like Ce [37] and Pr [38], have been discussed in the framework of the Anderson-Impurity model [49] where correlation effects are taken into account to explain the results. There is especially no indication that correlation effects need to be taken into account to explain the observations.

II) Planer and apical sites in strontium ruthinate

The next example is an illustration of how x-ray photoemission spectroscopy (XPS), used in conjunction with XES and computational aids, elucidates the electronic properties of an important superconducting compound, Sr_2RuO_4, which is the first copperless oxide superconductor having a layered Perovskite structure. The electronic structure of Sr_2RuO_4 has been studied intensively during the last few years [50-57]. This material has the same crystal structure as La_2CuO_4 with RuO_2 planes replacing the CuO_2 planes. As with the cuprates, the resistivity in-plane and perpendicular to the plane is highly anisotropic. On the other hand, there are differences between Sr_2RuO_4 and high-T_c superconductors. High temperature superconductors such as Sr_2RuO_4 are superconducting without any chemical doping. The d orbitals involved in hybridization with oxygen 2p states are different; they are of the t_{2g} type (d_{xy}, d_{xz}, d_{yz}) in Sr_2RuO_4 and of the e_g type ($d_{x^2-y^2}$) in copper oxides. The perovskite, Sr_2RuO_4, shows an enhanced Pauli paramagnetism, while La_2CuO_4 is an antiferromagnetic insulator. In spite of several band structure calculations of

Sr_2RuO_4[50-52] only a few ultraviolet photoelectron emission (UPS) [55], XPS [57], and angle-resolved photoemission [53,54] spectral measurements are available.

Our work [41] on this compound is an x-ray emission spectral study of selectively excited Ru $N_{2,3}$ (4d→4p transition) and O Kα (2p→1s transition). The measurements of O Kα x-ray emission spectra near the O 1s threshold were performed at the Advanced Light Source, while the measurements of Ru $N_{2,3}$ XES at hν=200 eV and O 1s total fluorescence yield (TFY) spectra were performed on the BL-19B undulator beam line [58] of the Photon Factory located at the National Laboratory for High Energy Physics (KEK) in Japan.

The soft x-ray absorption spectrum of Sr_2RuO_4 measured near the O K-edge using TFY detection is given in Fig. 3(a). The results are similar to O 1s near edge x-ray absorption fine structure measurements [55] of Sr_2RuO_4. According to band structure calculations of Singh [51] [reproduced in Fig. 3b)], one can attribute the origin of peak *A* at hν ~528.5 eV to a transition of an O 1s electron to the O(1) 2p in-plane unoccupied states (A') just above the Fermi energy. From the calculations presented in Fig. 3(b), the O(2) 2p apical density of states (DOS) contribution is very small in the region extending a few eV above the Fermi energy but reaches a maximum about five eV above the threshold. Thus, we can attribute feature B and C in the O 1s TFY spectrum located at hν ~530 and 531.5 eV, respectively, to a comparable mixture of O(1) and O(2) 2p states [*B'* and *C'* in Fig. 3(b)]. From Fig. 3(b) we observe the increasing contribution to the O(2) 2p apical state (*D'*) and interpret the increasing fluorescence at hν ~533.5 eV labeled D in Fig. 3(a) to these O(2) 2p apical states. As the excitation energy continues to increase, the O(1) 2p channel shows an increasing density of states at *E'* about 8 eV above the threshold. This increase can be described as a mixing of unoccupied O(1) and O(2) 2p states in the O 1s TFY-spectrum between 536 and 540 eV shown in Fig. 3(a).

Fig. 4(a) shows the O Kα XES (2p→1s transition) of Sr_2RuO_4 recorded at selected excitation energies indicated by the vertical lines in Fig. 3(a). Oxygen Kα x-ray emission probes the valence band states with p-symmetry. As the excitation energy increases, the prominent feature at hν=523 eV is reduced to a shoulder in the spectra obtained at photon energies greater than about 533 eV. At the excitation energy hν ~534 eV, the O Kα XES valence spectrum is a narrower and more symmetrical band. This spectrum is quite different with respect to that obtained at hν ~529.2 eV.

The extremely high sensitivity of the O Kα XES to excitation energy can be attributed to the significant differences between in-plane [O(1)] and out-of-plane apical [O(2)] 2p DOS in Sr_2RuO_4. We can check this suggestion by comparing the XES spectrum obtained from mostly O(1) in-plane atoms (hν=529.2) with the spectrum obtained from the apical O(2) sites (hν=534.2) with LDA

band structure calculations [51-53], which are reproduced in the upper panels of Fig 4(b). The distribution of O(1) 2p DOS has an extended two-peak character, as indicated by the broadened DOS shown as the dashed curve. For the apical O(2) 2p states, the center of gravity of the DOS is shifted toward the top of the valence band and is much narrower as can be seen by the broadened DOS in the lower panels of Fig. 4(b).

The calculations can be compared to the experimental O Kα XES of Sr_2RuO_4 taken at an energy of 529.2 eV, which probes primarily the in-plane O(1) DOS. The broad emission spectrum with two distinct features suggests that the emission is primarily from O(1) in-plane atoms as is also confirmed by the calculations. Comparing the O Kα emission spectrum at 534.2 eV which is primarily due to O(2) apical sites as probed by the absorbing photons, we see the emission spectrum is much sharper showing the single peak and a weak shoulder reproduced by the calculations for that site in Fig. 4(b). The complimentary nature of the XES, TFY, and the calculations lead us to differentiate the emission produced by the oxygen atoms at the two different sites. We now wish to place these spectra on a binding energy scale along with the emission from the ruthenium atoms in order to evaluate the O-Ru bonding.

The XPS spectrum of Sr_2RuO_4 at the O 1s core level consists of two lines separated by ~0.8 eV [57], which corresponds to the different O 1s binding energies (b.e.) for the O(1) and O(2) atoms occupying non-equivalent positions. A similar difference (ΔE =1.45 eV) of O 1s b.e. for O(1) and O(2) atoms is predicted by the band structure calculations of Singh [51]. We have inferred that the O Kα XES of Sr_2RuO_4 measured at E~534.2, as shown in Fig. 4(a) is similar to the calculated O(2) 2p DOS of Sr_2RuO_4 shown in Fig. 4(b), while the O Kα XES of Sr_2RuO_4 selectively excited at 529.2 eV shows mostly the in-plane O(1) DOS. The high-energy tail seen in that spectrum can be attributed to the increased DOS at the O(1) site found at b' in the calculations. At excitation energies about 544 eV, the O Kα XES of Sr_2RuO_4 can be simulated by a superposition of spectra corresponding to a linear combination of the O(1) 2p and O(2) 2p DOS.

The O Kα emission from Sr_2RuO_4 is adjusted to the binding energy scale using O 1s XPS binding energy data. In Fig. 5 the emission bands of Ru $N_{2,3}$ [58] are compared to the O(1) and O(2) Kα emission bands and with the UPS spectrum of Sr_2RuO_4 excited at hν=21.[57] If one estimates the values of the photoionization cross sections of O 2p and Ru 4d-states obtained from Ref.59, one can conclude that UPS spectra excited at 21 eV probes both Ru 4d and O 2p states. Furthermore, O Kα and Ru $N_{2,3}$ XES probes O 2p and Ru 4d states directly because of the dipole selection rules (2p→1s and 4d→4p transitions, respectively). We note that the energy position of the subband of O Kα XES excited at hν=529.2 eV coincides with the peak of the UPS spectrum

located at 5.7 eV in Fig. 5. The intensity maximum of O Kα XES excited at 534.2 eV (corresponding mostly to the DOS of the O(2) apical sites) does not coincide well with the UPS peak located at 2.6 eV or at 5.7 eV. This strongly suggests that O Kα XES excited at 534.2 eV has some contribution of O (1) 2p states but isn't strongly hybridized.

The intense peak of Ru $N_{2,3}$ XES located at 6 eV binding energy coincides closely to the O Kα XES subband excited at 529.2 eV. This suggests that Ru 4d states are mostly hybridized with O(1) 2p in-plane states, which agrees with band structure calculations [50-52]. According to angle-resolved photoemission measurements of Sr_2RuO_4 [54], these Ru 4d-states are derived from d_{xy}, d_{xz} and d_{yz}-orbitals. From the classification given in Ref. 60, one can conclude that O(1) 2p states which are mixed with Ru $4d_{xy,xz,yz}$-states form p bonds, which also is consistent with the LDA band structure calculations [50-52]. Our measurements have provided additional evidence that the p orbits of the oxygen in-plane atoms bond strongly with d_{xy},d_{yz},d_{zx} Ru orbits of Sr_2RuO_4 [61].

These results are a demonstration of how one can selectively excite specific oxygen sites by tuning the excitation energy because the O 1s absorption cross section between in-plane and apical oxygen atoms is different. Our results also show that the O Kα XES spectra are in a good agreement with band structure calculations, and one can obtain information about the Ru and O bonds. Finally the discrepancy with the intensity distribution of the Ru $N_{2,3}$ XES compared to the LDA calculations suggests that possibly a local two-hole-like final state due to one-site Coulomb correlations produces an enhanced density of states at 6 eV binding energy.

ACKNOWLEDGMENTS

We are grateful to Dr.D.Singh, Dr.T.Oguchi and Dr.I.Hase for making available the full data of their band structure calculations, and Dr. M. Matteucci for participation in measurements and discussion. This work was supported by NSF Grants (No. DMR-901 7997 and No. DMR-9420425) and the DOE EPSCOR and Louisiana Education Quality Special Fund (Grant No. DOE-LEQSF (1993-95)-03) and the U.S. DOE, BES (Contract No. W-31-109-Eng-38). The Russian State Program on Superconductivity (project 95026), Russian Science Foundation for Fundamental Research (Projects N 96-03-3209 and 96-15-96598), and a NATO Linkage Grant. The work at the Advanced Light Source at Lawrence Berkeley National Laboratory was supported by U.S. Department of Energy (Contract No. DE-AC03-76SF00098).

REFERENCES

1) W. C. Röntgen, (Trans. by A. Stanton) Nature **53**, 274 (1896).
2) A. H. Compton, and S.K. Allison, *X-Rays in Theory and Experiment* (D. Van Nostrand Co, New York, 1935).
3) L. G. Parratt, Rev. Mod. Phys. **31**, 616 (1959).
4) D. H. Tomboulian, *Handbuch der Physik*, Vol. **XXX** S.Flügge/Marburg, Editors (Springer-Verlag, Berlin, 1957) pp. 246-304.
5) D. L. Ederer, T. A. Callcott, and R. C. C. Perera, Synchrotron Radiation News, **7**, 29 (1994).
6) D. L. Ederer, J. A. Carlisle, J. Jimenez-Mier, J. J. Jia, K. Osborn, T. A. Callcott, R. C. C. Perera, J. H. Underwood, L. E. Terminello, A. Asfaw, and F. J. Himsel, J. Vac. Sci. Technol. A **14**, 859 (1996).
7) *Handbook for Synchrotron Radiation,* Series Editors, H. Winick and T. Sasaki (North Holland, Amsterdam, 1991).
8) Proceedings of the Workshop: *Raman Emission by X-Rays* , D.L. Ederer, and J.H. McGuire, Editors (World Scientific Publishing, Singapore, 1996).
9) *Resonant Anomalous X-Ray Scattering: Theory and Applications,* G. Materlik, C. J. Sparks, and K. Fischer, Editors (North Holland, Amsterdam 1994).
10) P. P. Kane, Radiat. Phys. Chem. **50**, 31 (1997).
11) Y. Ma, Synchrotron Radiation News, **8**, 26 (1995).
12) S. Shin, Synchrotron Radiation News, **8**, 16 (1995).
13) T. Hayashi, M. Suzuke, and Y. Hayashi, The Science Reports of the Tohoku University, **LII**, 57 (1969).
14) C. J. Sparks, Phys. Rev. Lett. **33**, 262 (1974).
15) P. Eisenberger, P. M. Platzman, and H. Winick, Phys. Rev. Letts. **36**, 623 (1976).
16) J. P. Briand, D. Girard, V. O. Kostroum, P. Chevalier, K. Wohrer, and J. P. Mossé, Phys. Rev. Lett. **46**, 1625 (1981).
17) See e.g. J.J. Sakurai, Advanced Quantum Mechanics (Addison-Wesley, Reading, MA, 1967), Chap. 2 and T. Aberg, Phys. Scr. **21**, 495 (1980), J. Tulkki and T. Aberg, J. Phys.B **15**, L 435 (1982).
18) T. Åberg, T. and J. Tulkki, *Atomic Inner Shell Physics*, Bernd Crasemann Editor (Plenum Publishing Corp., New York, 1985) p. 419.
19) P. Cowan, *Resonant Anomalous X-ray Scattering: Theory and Applications*, G. Materlik, C. J. sparks, and K Fischer, Editors (Elsevier Science B.V., Amsterdam, 1994) p. 449.
20) Y. Ma, N. Wasshahl, P. Skytt, J. Guo, J. Nørdgren, P. D. Johnson, J.-E. Rubensson, T. Boske, W. Eberhardt, and S. D. Kevan, Phys. Rev. Lett. **69**, 2598 (1992).

21) K. E. Miyano, D. L. Ederer, T. A. Callcott, W. L. O'Brien, J. J Jia, L. Zhou, Q.-Y. Dong, Y. Ma, J. C. Woicik, and D. R. Mueller, Phys. Rev. **B48**-I, 1918 (1993).

22) J.-E. Rubensson, D. R. Mueller, R. Shuker, D. L. Ederer, C. H. Zhang, J. J. Jia, and T. A. Callcott, Phys. Rev. Lett. **64**, 1047 (1990).

23) S. Shin, A. Agui, M. Watanabe, M. Fujisawa, Y. Tezuka , and T. Ishii, Phys. Rev. B **53**, 15660 (1996).

24) J. A. Carlisle, E. L. Shirley, E. A. Hudson, L. E. Terminello, T. A. Callcott, J. J. Jia, D. L. Ederer, R. C. C. Perera, and F. J. Himsel, Phys. Rev. Lett. **74**, 1234 (1995).

25) J. J. Jia, T. A. Callcott, E. L. Shirley, J. A. Carlisle, L. Terminello, A. Asfaw, D. L. Ederer, F. J. Himpsel, and R. C. C. Perera, Phys. Rev. Lett. **76**, 4054 (1996).

26) J. J. Jia, T. A. Callcott, D. L. Ederer, R. C. C. Perera, J. of Electr. Spectr. Rel. Phen. **92**, 181 (1998).

27) S. Shin, M. Fujisawa, H. Ishii, Y. Harada, M. Watanabe, M. M. Grush, T. A. Callcott, R. C. C. Perera, E. Z. Kuramev, A. Moewes, R. Winarski, S. Stadler, and D. L. Ederer, J. of Electr. Spectr. Rel. Phen. **92**, 197 (1998).

28) E. D. Isaacs, P. M. Platzman, P. Medcalf, and J. M. Honing, Phys. Rev. Lett. **76**, 4211 (1996).

29) J. Jiménez-Mier, D. L. Ederer, U. Diebold, A. Moewes, T. A. Callcott, L. Zhou, J. J. Jia, J. Carlisle, E. Hudson, L. Terminello, A. Asfaw, F. J. Himpsel, and R. C. C. Perera, in *Raman Emission by X-Ray Scattering*, D. L. Ederer and J. H. McGuire, eds. (World Scientific, Singapore, 1996) p. 71.

30) S. M. Butorin, J.-H. Gou, M. Magnuson, and J. Nordgren, Phys. Rev. B **55**, 4242 (1997).

31) Y. Uehara, D. W. Lindle, T. A. Callcott, L. T. Terminello, F. J. Himpsel, D. L. Ederer, J. H. Underwood, E. M. Gullikson, and R. C. C. Perera, Appl. Physics A **65**, 179 (1997).

32) S. M. Butorin, J.-H. Guo, M. Magnuson, P. Kuiper, and J. Nordgren, Phys. Rev. B **54**, 4405 (1996).

33) E. Z. Kurmaev, M. A. Korotin, V. R. Galakhov, L. D. Finkelstein, E. I. Zabolotzky, N. N. Efremova, N. I. Lobachevskaya, S. Stadler and D. L. Ederer, T. A. Callcott and L. Zhou, A.Moewes, S. Bartkowski and M. Neumann, J. Matsuno, T. Mizokawa, A. Fujimori, and J. Mitchell, submitted to Phys. Rev. B (1998).

34) P. Kuiper, J.-H. Guo, C. Såthe, L.-C. Duda, and J. Nordgren, J. J. M. Pothuizen, F. M. F. de Groot, and G. A. Sawatzky, Phys. Rev Lett. **80**, 5204 (1998).

35) A. Moewes, T. Eskildsen, D. L. Ederer, J. Wang, J. McGuire, T. A. Callcott, Phys. Rev. B **57**, R8059 (1998).

36) J.-J. Gallet, J.-M. Mariot, C. F. Hague, F. Sirotti, M. Nakazawa, H. Ogasawara, and A. Kotani, Phys. Rev. B **54**, R14238 (1996).

37) S. M. Butorin, D. C. Mancini, J.-H. Guo, N. Wassdahl, J. Nordgren, M. Nakazawa, S. Tanaka, T. Uozumi, A. Kotani, Y. Ma, K. E. Myano, B. A. Karlin, and D. K. Shuh, Phys. Rev. Lett. **77**, 574 (1996).

38) S. M. Butorin, L.-C. Duda, J.-H. Guo, N. Wassdahl, J. Nordgren, M. Nakazawa, and A. Kotani, J. Phys.: Condens. Matt. **9**, 8155 (1997).

39) A. Moewes, S. Stadler, R. P. Winarski, D. L. Ederer, M. M. Grush, and T. A. Callcott, accepted for publication in Phys. Rev. B.

40) A. Moewes, S. Stadler, R. P. Winarski, D. L. Ederer, M. M. Grush, and T. A. Callcott, accepted as a Rapid Communication in Phys. Rev. B. **51** (1998).

41) E. Z. Kurmaev, S. Stadler, D. L. Ederer, Y. Harada, S. Shin, M. M. Grush, T. A. Callcott, R. C. C. Perera, D. A. Zatsepin, N. Ovechkina, M. Kasai, Y. Tokura, T. Takahashi, K. Chandrasekaran, R. Vijayaraghavan, and U. V. Varadaraju, Phys. Rev. B **57**, 1558 (1998).

42) T. A. Callcott, K. L. Tsang, C. H. Zhang, D. L. Ederer, and E. T. Arakawa, Rev. Sci. Inst. **57**, 2680 (1986).

43) J. Nordgren, G. Bray, S. Cramm, R. Nyholm, J.-E. Rubensson.and N. Wassdahl, Rev. Sci. Instrum. **60**, 1690 (1989).

44) J. J. Jia, T. A. Callcott, J. Yurkas, F. J. Himsel, M. C. Samant, J. Stöhr, D. L. Ederer, J. A. Carlisle, E. A. Hudson, L. J. Terminello, R. C. C. Perera, and, D. K. Shuh, Rev. Sci. Instrum. **66**, 1394 (1995).

45) A. Asfaw, D. L. Ederer, L. Zhou, L. Lin, K. Osborn, T. A. Callcott, K. E. Miyano, E. Morikawa, Rev. Sci. Instrum. **66** (2), 1627 (1995).

46) R.D. Cowan, *The Theory of Atomic Structure and Spectra*, (University of California Press, Berkeley, 1981).

47) H. Ogasawara and A. Kotani, J. Phys. Soc. Jpn **64**, 1394 (1995).

48) M. Okusawa, K. Ichikawa, O. Aita, and K. Tsutsumi, Phys. Rev. B **35**, 478 (1987).

49) O. Gunnarson and K. Schönhammer, Phys. Rev. B **28**, 4315 (1983).

50) T.Oguchi, Phys. Rev. B **51**, 1385 (1995)

51) D. J. Singh, Phys. Rev. B **52**, 1358 (1995)

52) I. Hase and Y. Nishihara, J. Phys. Soc. Jpn. **65,** 3965 (1996)

53) T. Yokoya, A.Chainani, T. Takahashi, H. Katayama-Yoshida, M. Kasai, and Y. Tokura, Phys. Rev. Lett. **76**, 3009 (1996) ; T. Yokoya, A. Chainani, T. Takahashi, H. Ding, J. C. Campuzano, H. Kotayama-Yoshida, M. Kasai, and Y. Tokura, Phys. Rev. B **54** , 13311 (1996)

54) D. H. Lu, M. Schmidt, T. R. Cummins, S. Schuppler, F. Lichtenberg, and J. G. Bednorz, Phys. Rev. Lett. **76**, 4845 (1996).
55) M. Schmidt, T. R. Commins, M. Bürk, , D. H. Lu, N. Nücker, S. Schuppler, and F. Lichtenberg, Phys. Rev. B **53**, R14761 (1996).
56) G. Baskaran, Physica B **223 & 224**, 490 (1996).
57) T. Yokoya, A. Chainani, T. Takahashi, H. Kotayama-Yoshida, M. Kasai, Y. Tokura, N. Shanthi, and D. D. Sarma, Phys. Rev. B **53**, 8151 (1996).
58) M. Fujisawa, A. Harasawa, A. Agui, M. Watanasbe, A. Kakizaki, S. Shin, T. Ishii, T. Kita, T. Harada, Rev. Sci. Instrum. 67, **345** (1996).J. J. Yex and I. Lindau, At. Data Nucl. Data Tables **32**, 1 (1985).
59) J. J. Yea, and I. Lindau, At. Data Nucl. Data Tables **32**, 1 (1985).
60) L. F. Mattheiss, Phys. Rev. B **13,** 2433 (1976).
61) L. F. Mattheiss and D. R. Hamann, Phys. Rev. B **40**, 2217 (1989)

TABLE I

A partial listing of recent measurements of resonant Raman scattering in 3d transition metals and rare earths.

Material/Element (3d Transition Metals)	Raman Loss (eV)	Comments	Ref.
CaF_2	16.5	Raman band mimics the valence band	26
Sc oxides and halides	6.1-14.4	Raman loss variable depends on reactivity of anion	27
$SrVO_3$	1	d-d transition in V band	27
	6.8	O 2p to C band	27
V_2O_5	6.2	d^0 therefore no d-d?, O 2p to C band	27
V_2O_3	13	Metallic phase	28
V_2O_3	10 and 13	AFI insulating phase	28
Ti (metal)	3.8	d-d transition	29
	2.1	Multielectron excitation	29
TiO	4.2	d-d transition	29
	2.4	Multielectron excitation	29
TiO_2	7.9	d-d transition	29
	23.1	O 2p to C band	29
	2.1	Multielectron excitation	29
TiO_2	7.9	d-d transition	29
$BaTiO_3$	14.1	d-d transition	29
	22.5	O 2p to C band	29
	7.6	Multielectron excitation	29
TiO_2	8	d-d transition	30
$FeTiO_2$	7.5	d-d charge transfer	30
$KMnO_4$	7.5	" " "	30
$BaSrTiO_3$	6	d-d transition	31
	Dispersive	Features in VB emission associated with C-K tran.	31
MnO	4	d-d transition	32
$Pr_{0.5}Sr_{0.5}MnO_3$	2	" " "	33
	7	d-d transition with charge transfer	33
$Sr_2CuO_2Cl_2$	1.5	Polarization dependent d-d transitons	34
	1.7	" " " "	34
(Rare Earths)			
$(Y,Gd)_2O_3$	3.8	Excitations within the 4f shell, ie: f-f transitions	35
	4.3	" " " "	35
	4.8	" " " "	35
	5.8	" " " "	35
Gd	27	5p-4f net transition	36
CeO_2	6	f-f transition with charge transfer	37
Pr O_2	4	" " " "	38
Nd_2O_3	2.3	" " " "	39
	21	5p-4f net transition	39
$LaAlO_3$	7.5	f-f transition with charge transfer	40
	16.3	5p-4f net transition	40

FIGURE CAPTIONS:

FIG. 1. Soft x-ray emission spectrum (XES) excited above the 3d-4f threshold, total electron yield spectrum (TEY), partial fluorescence yield (PFY) of Nd_2O_3 and calculated transitions for atomic Nd in the vicinity of the 3d-4f threshold.

FIG. 2. Soft x-ray emission spectra of Nd_2O_3 excited in the region of the 3d - 4f threshold. The excitation energy for the spectra is given above each spectrum.

FIG. 3. (a) The x-ray total fluorescence yield of Sr_2RuO_4 near O K- edge. The photon energy (abscissa) is adjusted to the energy scale in (b) for ease of comparison by aligning peaks labeled A in (a) and (b) in the figure.
(b) The results of band structure calculations of Sr_2RuO_4. The energy scale (abscissa) is scaled relative to the bottom of the conduction band from the calculation. (adapted from Ref. 41).

FIG.4. (a) The experimental O Kα XES of Sr_2RuO_4 measured at different excitation energies.
(b) O(1), O(2) 2p density of states distribution taken from LDA band structure calculations of Sr_2RuO_4 by Oguchi [51], Singh, [52] and Hase [53] (adapted from Ref. 41).

Fig. 5. The comparison of the experimental Ru $N_{2,3}$ XES (measured at E=200 eV), O Kα XES (measured at E=529.2 and 534.2 eV) with UPS of Sr_2RuO_4 excited at E=21 eV. (adapted from Ref. 41).

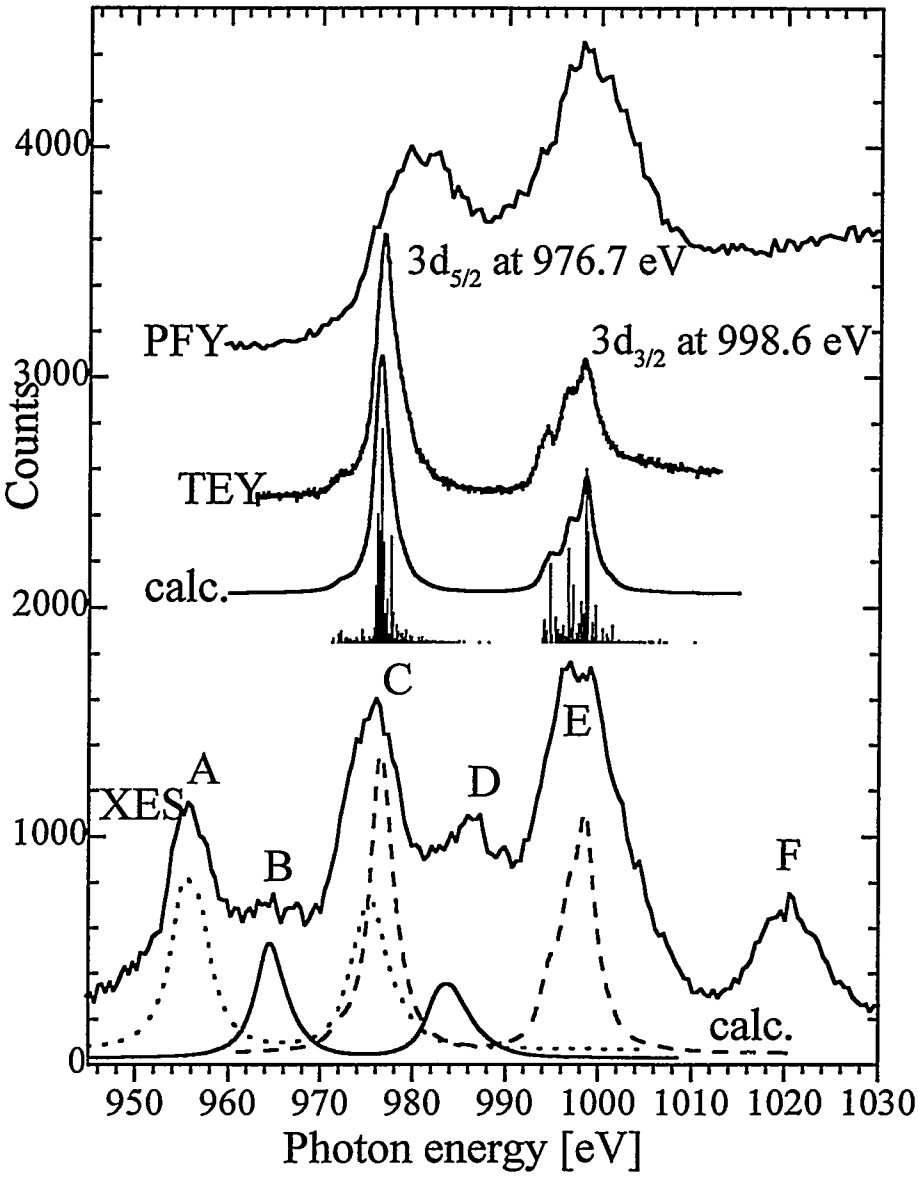
4000
3000
2000
1000
0
Counts
PFY
TEY
calc.
3d5/2 at 976.7 eV
3d3/2 at 998.6 eV
XES
A
B
C
D
E
F
calc.
950
960
970
980
990
1000
1010
1020
1030
Photon energy [eV]

Fig 1

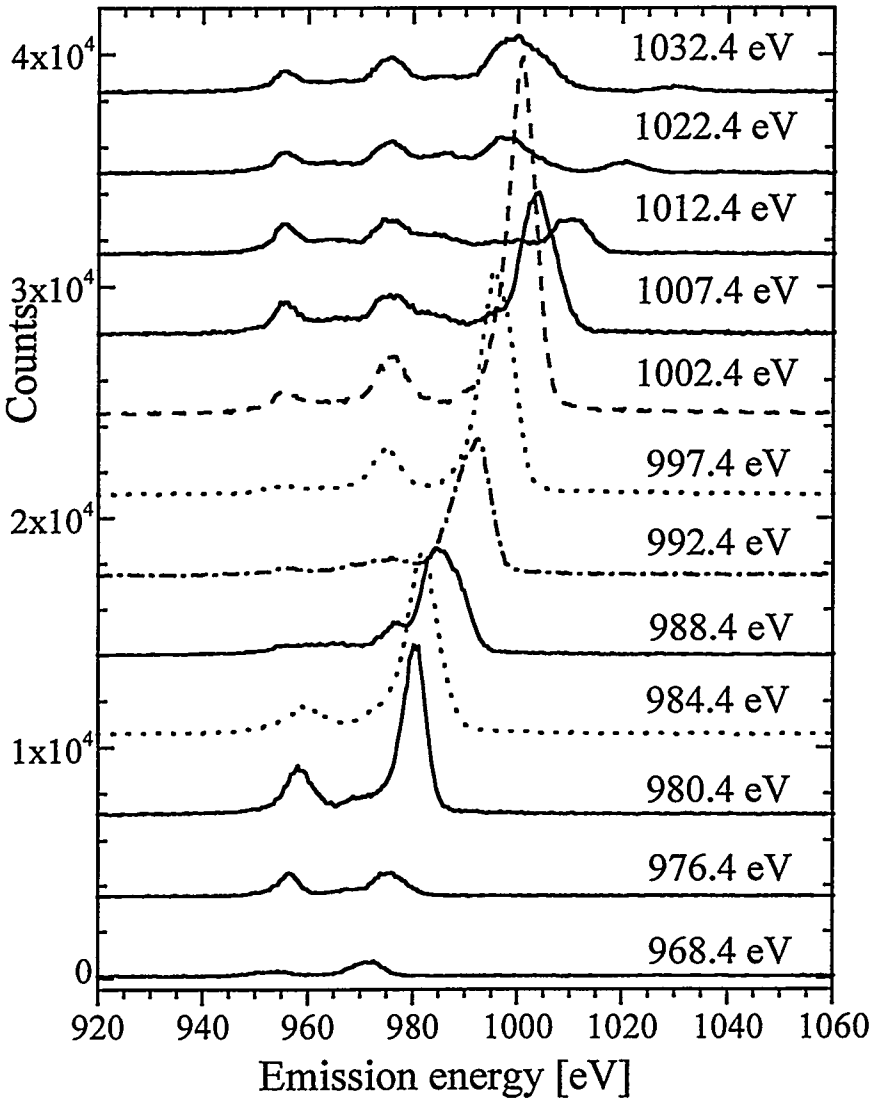
4x10^4
3x10^4
2x10^4
1x10^4
0
Counts
1032.4 eV
1022.4 eV
1012.4 eV
1007.4 eV
1002.4 eV
997.4 eV
992.4 eV
988.4 eV
984.4 eV
980.4 eV
976.4 eV
968.4 eV
920
940
960
980
1000
1020
1040
1060
Emission energy [eV]

Fig 2

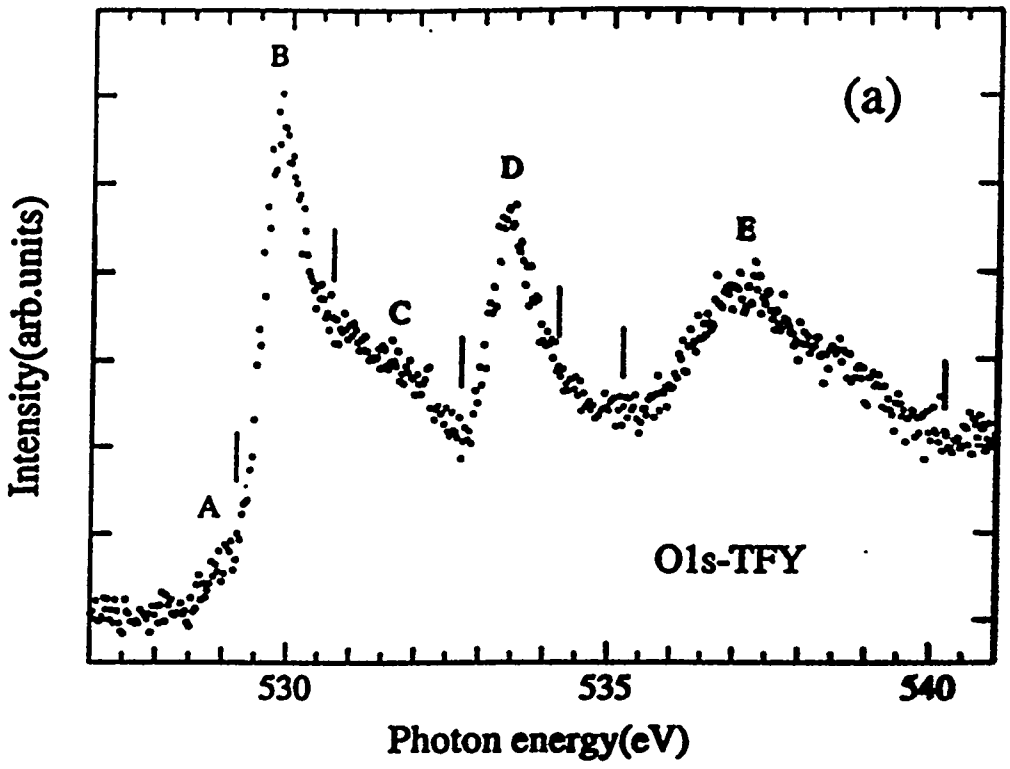
(a)
B
D
E
C
A
O1s-TFY
Intensity(arb.units)
530
535
540
Photon energy(eV)

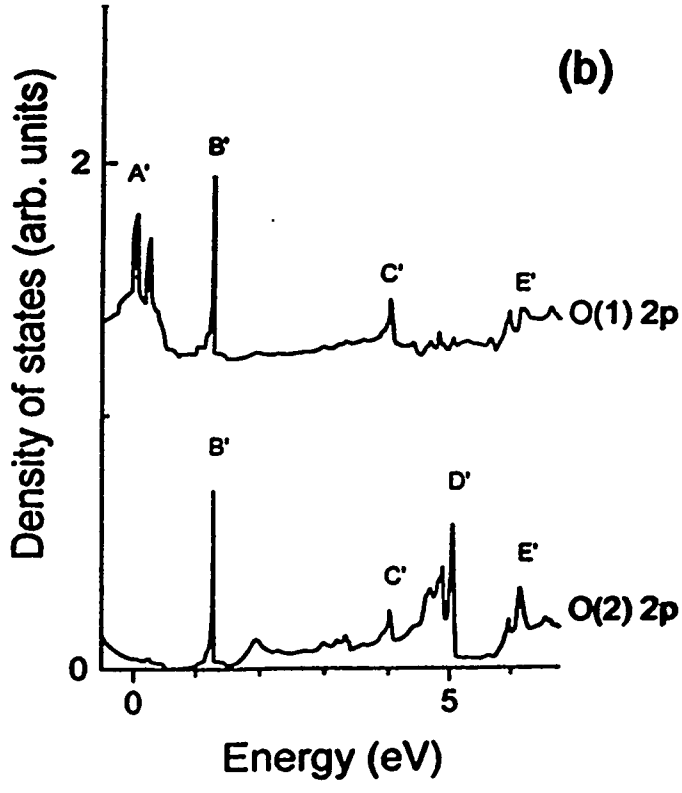
(b)
A'
B'
C'
E'
O(1) 2p
B'
D'
C'
E'
O(2) 2p
Density of states (arb. units)
2
0
0
5
Energy (eV)

Fig 3

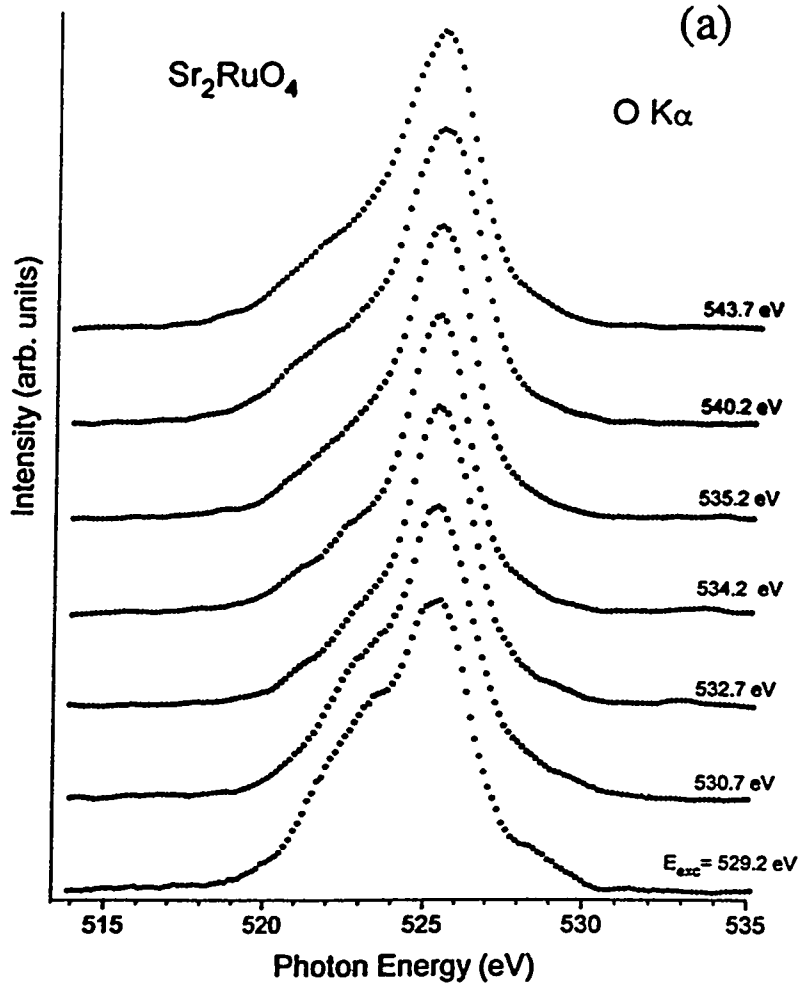
(a)
Sr_2RuO_4
O Kα
543.7 eV
540.2 eV
535.2 eV
534.2 eV
532.7 eV
530.7 eV
E_{exc}= 529.2 eV
Intensity (arb. units)
515
520
525
530
535
Photon Energy (eV)

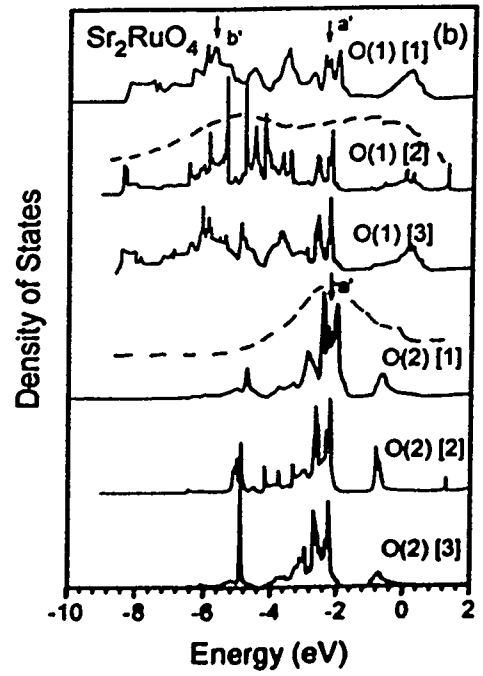
Sr_2RuO_4
b'
a'
O(1) [1]
(b)
O(1) [2]
O(1) [3]
O(2) [1]
O(2) [2]
O(2) [3]
Density of States
-10
-8
-6
-4
-2
0
2
Energy (eV)

Fig 4

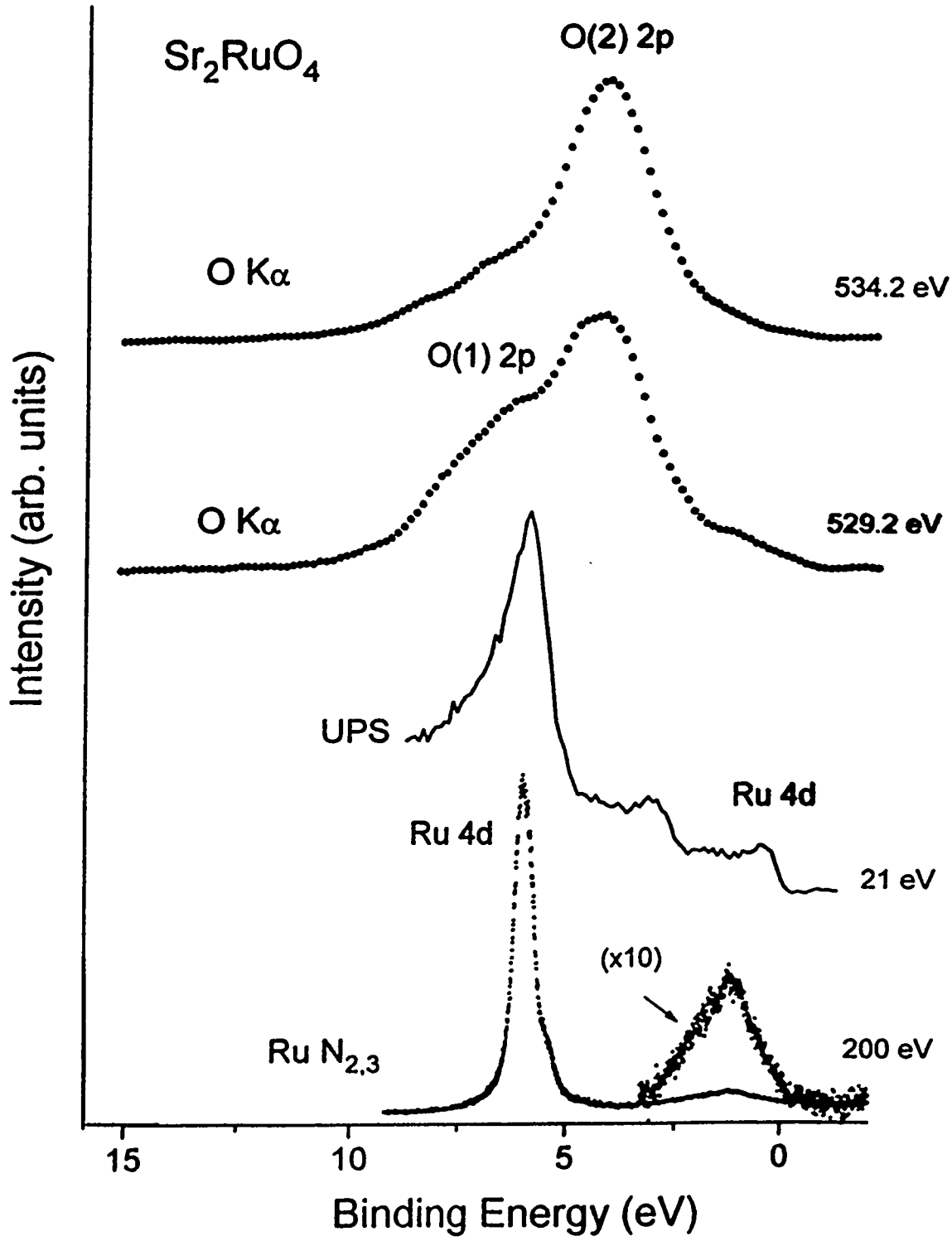
Sr_2RuO_4
O(2) 2p
O Kα
534.2 eV
O(1) 2p
O Kα
529.2 eV
UPS
Ru 4d
Ru 4d
21 eV
(x10)
Ru $N_{2,3}$
200 eV
Intensity (arb. units)
15
10
5
0
Binding Energy (eV)

Fig 5